ACSNANO

www.acsnano.org

ARTICLE

Monolayer WS_2 Lateral Homosuperlattices with Two-dimensional Periodic Localized Photoluminescence

Wanli Yang, Tiantian Huang, Junbo He, Shuaijun Zhang, Yan Yang, Weiming Liu, Xun Ge, Rui Zhang, Mengxia Qiu, Yuxiang Sang, Xingjun Wang, Xiaohao Zhou, Tianxin Li, Congfeng Liu, Ning Dai, Xin Chen,* Zhiyong Fan,* and Guozhen Shen*

Cite This: https://doi.org/10.1021/acsnano.1c07803

Read Online

ACCESS | Metrics & More | Article Recommendations | Supporting Information

ABSTRACT: **Homojunctions and homosuperlattices are essential structures and have been widely explored for use in advanced electronic and optoelectronic devices. However, artificially manipulating crystalline phases in two-dimensional (2D) monolayers is still challenging, especially when attempting to engineer lateral homogeneous junctions in a single monolayer of transition metal dichalcogenides (TMDs). Herein, we demonstrate a lateral homosuperlattice (MLHS) with alternating 1T and 2H domains in a 2D WS_2 monolayer plane. In MLHSs, the 2H domains, which are laterally localized and isolated by potential wells, manifest junction interfaces and irradiated photoluminescence (PL) with a lateral periodic distribution in the two-dimensional plane. The studies on MLHSs here can provide further understanding of lateral homojunctions and homosuperlattices in a monolayer plane, providing an alternative route to modulate optical and electronic behaviors in TMD monolayers.**

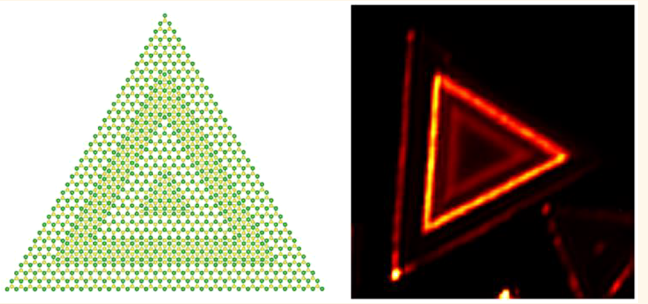

KEYWORDS: *WS_2, homosuperlattices, 1T and 2H phases, potential wells, photoluminescence*

Homojunctions, heterojunctions, and correlated superlattices are fundamental elements in modern photonics and electronics.[1−4] Dense integration, obtaining superlative performance, and downscaling remain pressing challenges for homo/heterojunction devices. Recently, 2D homo/heterostructures (*e.g.*, graphene, TMDs) have shown great potential in the fields of physical research and advanced optoelectronic devices.[2−10] Specifically, artificial manipulations of the crystalline phases and superlattices of 2D materials have been successfully exploited to produce devices with better integration[10,11] and performance.[1−4,7−9,12−16] TMDs stacking structures have been used to realize high carrier mobility and rapid on/off response in functional materials and devices. However, in spite of the progress made, it is still challenging and of the utmost necessity to control the integration precisely, inner interfaces, and band offsets of lateral and vertical homogeneous structures.[2,7,13] Aiming at these goals, many efforts have been made on thickness modulation, doping, and phase engineering[13,14,17−21] to realize lateral homojunctions,[22] composition-dependent phase variations,[23] and ohmic homomorphic contacts.[24]

Phase engineering is a well-known and robust way to effectively modulate the lattices and physical properties (*e.g.*, band structure and phonon vibration) of homostructural materials.[25,26] Nevertheless, it is still urgent in the 2D community to understand and explore 2D lateral homojunctions and superlattices on the horizontal plane. Existing strategies, including ion intercalation,[13] laser irradiation[18,24] and electron beam induction,[19] have been used to engineer TMD homostructures. To the best of our knowledge, few attempts have been made to achieve difficult engineering of 2D monolayer lateral homosuperlattices (MLHSs), where various arranged phases spontaneously form in a monolayer plane of TMDs. Herein, we demonstrate a MLHS with alternating 1T and 2H phases in a WS_2 single layer. The MLHSs demonstrate

Received: September 6, 2021
Accepted: December 13, 2021

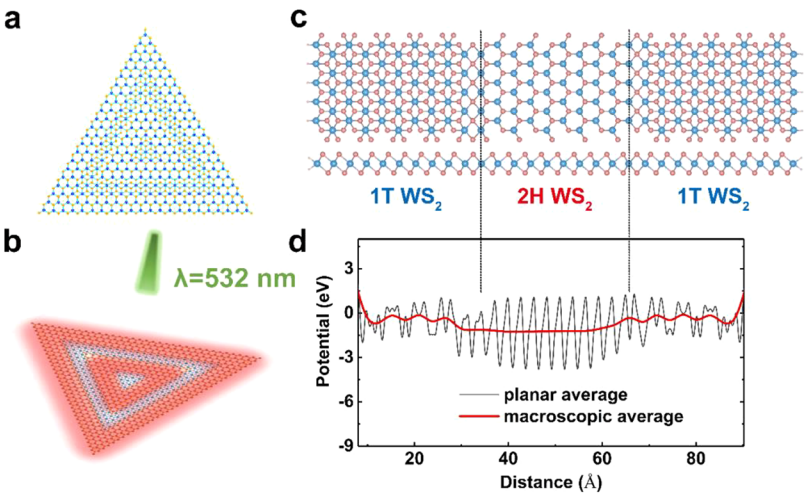

Figure 1. (a) Schematic showing two-dimensional MLHSs with 1T/2H-WS_2. (b) Schematic illustration of 1T/2H-WS_2 MLHSs irradiated with a 532 nm laser. (c) Atomic model and (d) potential distributions of an alternating lateral 1T-2H-1T construction in a WS_2 monolayer simulated with density functional theory.

a lateral periodic distribution of photoluminescence and junction interfaces originating from alternating arrangement of semiconductor phases (2H) and metal phases (1T) in the monolayer plane. The localized electrons in the 2H phases and the surface potential distributions lead to enhanced radiation recombination in the MLHSs with alternating 2H and 1T phases. The emergence of MLHSs in ML-WS_2 will provide a better in-depth understanding of 2D lateral homojunctions and associated optical and optoelectronic behaviors.

RESULTS AND DISCUSSION

Understanding and constructing lateral homojunctions and MLHSs in a monolayer is always a fundamentally challenging task. Figure 1 shows the concept and illustration of MLHSs with an alternating arrangement of the 1T phase and 2H phase in one WS_2 monolayer. Combined with covalent bonds in a WS_2 monolayer plane,[3,12,20] MLHSs can be regulated within the alternating 1T and 2H phases in a plane, and such construction in a monolayer of TMDs is also rarely explored. An atomic level schematic of MLHSs (Figure 1a) indicates that the trigonal prismatic structure (H-phase) and octahedral prismatic structure (T-phase) can form in TMDs according to the different coordination modes between transition metal atoms and chalcogenide atoms.[26−28] It is documented that semiconductor 2H-WS_2 exhibits a direct band gap and strong irradiated photoluminescence at room temperature because of the thickness of a single atomic layer.[29−32] In stark contrast, the metallic 1T phase in WS_2 shows a low work function and low contact resistance.[26,33,34] Thus, when MLHSs are irradiated with a 532 nm laser, there is a transverse periodic distribution of distinctive photoluminescence in a 2D monolayer, as shown in Figure 1b. In addition, the stronger photoluminescence occurring in the regions of the 2H-WS_2 phase in MLHSs is observed because the electrons are localized in the 2H-phase regions due to the quantum confinement effect and the potential well in MLHSs. Density functional theory (DFT) calculations were performed to further probe the presence of the potential well in MLHSs. There are potential differences between the different phases as known from previous reports.[35−38] An approximate model of 1T-2H-1T alternating nanoribbons in Figure 1c shows the formed potential wells in 2D MLHSs (Figure 1d). Thus, the theoretical calculation implies that the alternating 1T and 2H phases can produce a potential well in MLHSs.

In Figure 1, we have shown that the photoluminescence can be alternatingly distributed in space in a MLHS monolayer, which can be further confirmed by spectroscopy images. Figure 2 shows the optical microscopy photographs and PL intensity maps of various 2D MLHSs. Figure 2a displays a microscopy image of a WS_2 monolayer with another stacked bilayer in the center. We marked the layered WS_2 on a SiO_2/Si substrate with triangular regions using blue dashed lines and the bilayer in the center with a green dashed line. When this WS_2

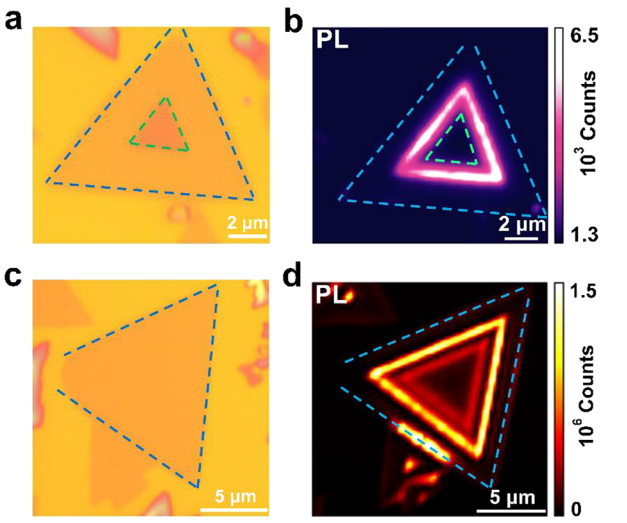

Figure 2. Various 2D MLHS configurations in different WS_2 monolayers. (a) Optical microscopy photographs in monolayer WS_2 with bilayer stacking on a SiO_2/Si substrate. (b) PL intensity mapping of the lateral homosuperlattices (LHSs) in (a). The green dashed triangle region in (a) and (b) is a bilayer and the region between the blue and green dashed triangles is a monolayer, while the highlighted region in (b) is 2H-WS_2. (c) Optical microscopy photographs of a WS_2 monolayer. (d) PL intensity mapping of MLHSs composed of 1T- and 2H-phase WS_2 on a SiO_2/Si substrate.

https://doi.org/10.1021/acsnano.1c07803
ACS Nano XXXX, XXX, XXX−XXX

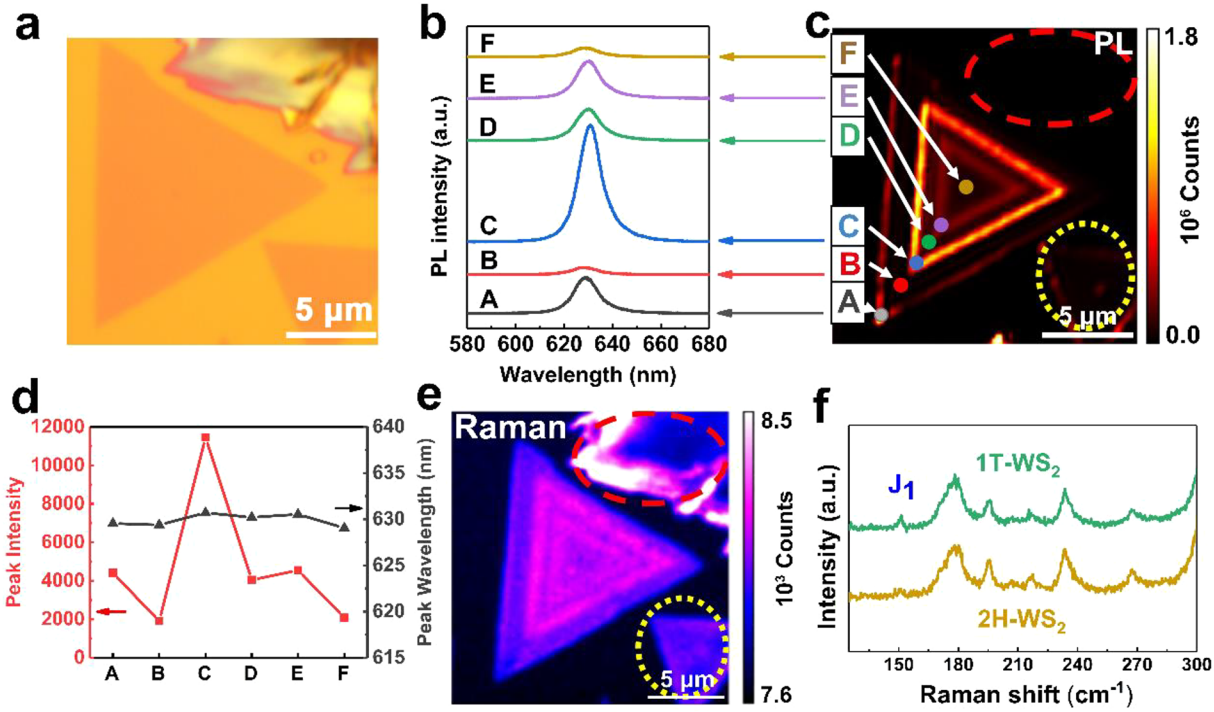

Figure 3. Raman and photoluminescence characterizations of a 2D MLHS with 1T/2H-WS_2 on a SiO_2/Si substrate. (a) Optical microscopy image. (b) Photoluminescence spectra of the A−F positions indicated in (c). (c) PL intensity map. (d) PL peak intensity profile (red) and the PL peak wavelength profile (black) from positions A to F in (b). (e) Raman intensity map corresponding to the PL map in (c). (f) Raman spectra of the 1T phase and 2H phase in monolayer WS_2.

monolayer was irradiated with a 532 nm laser, anomalous PL images were obtained, as shown in Figure 2b. Compared with the regions marked in green (*i.e.*, the stacked bilayer) in Figure 2a,b, we found that the bilayer region hardly exhibits a PL response. Such a phenomenon results from the bilayer.[39,40] Obvious PL only appears between the blue dashed lines and the green dashed line. Interestingly, the monolayer region shows an arranged PL distribution, which is different from the PL behaviors in monolayer WS_2.[29,41] As demonstrated in Figure 1, we believe that there is an alternating arrangement of 1T and 2H-WS_2 phases in the monolayer regions in Figure 2a. Moreover, the 2H-phase regions lie between two 1T-phase regions, which leads to such an arranged PL image due to the quantum confinement effect.[39,42]

To exclude the effect of the varying layer numbers, the WS_2 monolayer was also investigated, as shown in Figure 2c,d. No covered layer was observed in the WS_2 monolayer in the optical microscopy image in Figure 2c, while the PL intensity shows a similar arrangement in Figure 2d. The WS_2 MLHS involves five junctions where the bright regions should be 2H phases and the dark regions should be 1T phases. These results indicate that the triangle is positioned either on top of the superlattice or on the side and does not affect the formation and photoluminescence of such 2D MLHSs. This periodic and localized PL characteristic is dominated by the bilayer stacking, missing edge and edge defects of monolayer WS_2. Both the PL data and the theoretical calculations indicate that only the MLHS configuration results in such a PL arrangement in a single WS_2 monolayer, while ongoing exploration will focus on observing and controlling the microstructures in MLHSs.

To further verify the MLHS with 1T/2H-WS_2, we subsequently utilized Raman spectroscopy and PL spectroscopy to analyze the changes in this WS_2 monolayer. Figure 3a presents an optical micrograph of 2D MLHS with 1T/2H-WS_2, and the two layers are indistinguishable. It is worth mentioning that there is no observable optical contrast difference or thickness variation (*e.g.*, monolayer and bilayer) in the homosuperlattice, as shown in Figure 2a. This result affirms that WS_2 is homogeneous without a hybrid structure.[36,43] To delve more into the details, micro-PL spatial mapping is used to further investigate this homosuperlattice structure. Parts b and c of Figure 3 show the characteristic PL spectra and intensity map, respectively. In Figure 3c, the periodic PL image results from the regions of the alternating 1T and 2H phases that exist adjacently in monolayer WS_2. In addition, the corresponding PL spectra imply that there are obvious variations at positions A−F, as shown in Figure 3b. Furthermore, the special periodic localized photoluminescence of the MLHS in the 2D plane and the junction regions of the 1T and 2H phases exhibit abrupt boundaries, as can be seen from Figure 3c. The semiconducting 2H phase has a higher PL intensity, while the 1T phase has no obvious PL, as known from previous reports.[18] Thus, we observed and distinguished the difference between the 1T and 2H phases of WS_2 by the variations in the relative PL intensities in Figure 3c. In our cases, the clear contrast in the PL map provides further evidence of the existence of 1T and 2H phases and the formation of a homosuperlattice. Moreover, PL can provide a way to directly observe 2D MLHS with 1T/2H-WS_2 without any assistance from other measurement techniques. Figure 3d displays the changes in PL intensities at the different regions marked as A−F in Figure 3c. Strong PL intensities (in red) and peak wavelengths (in black) are found in regions A, C, and E, while there are no obvious PL intensities in regions B, D, and F. The red line profile (*i.e.*, PL intensities) shows that the PL intensities alternately change from positions A to F, and the C

https://doi.org/10.1021/acsnano.1c07803
ACS Nano XXXX, XXX, XXX−XXX

position has the strongest PL intensity. Additionally, the black line profile (*i.e.*, PL peak wavelength) does not obviously change and maintains a stable value of approximately 630 nm from points A to F.

In addition to PL mapping, Raman spectra were obtained to check and demonstrate that different phases existed in the WS_2 monolayer with alternating 1T and 2H phases.[33,36,43,44] Figure 3e shows the Raman intensity map using the WS_2 E_{2g}^1 mode at 350 cm^{-1}, revealing that the 1T and 2H regions had a regular variety of E_{2g}^1 intensities.[45] It is difficult to distinguish the 1T and 2H phases from the associated WS_2 E_{2g}^1 and A_{1g} position maps (seen in Supporting Information, Figure S1c,d), which insinuates that the flake is homogeneous. As documented elsewhere,[34,46] the J_1 mode in Figure 3f may be from the 1T phase, which can suggest the difference between the 1T and 2H phases. In addition, the regions marked by the yellow dashed circles show the contrast of the small WS_2 triangle, revealing weak PL emission, which mainly results from the 1T phase. The regions marked by red dashed circles are obvious in the Raman mapping (Figure 3e) but difficult to observe in the PL image (Figure 3c). This result indicates that such fantastic PL emission only occurs in a WS_2 monolayer with alternating 1T and 2H phases although other advanced measurements would also help observe and understand them. However, there are still a few alternating variations between B, D, F and A, C, E, implying that the 1T and 2H phases are positioned in the different domains separately rather than existing as an amalgam in one domain (see Supporting Information, Figure S1a).[43]

Neutral excitons and negative trions are often exploited to understand the fundamental behavior behind the PL emission in layered WS_2 materials. The behaviors of excitons generally dominate the optical properties and light emission of 2D semiconductor materials.[31,32,42,43] Figure 4a outlines the schematic illustration of the neutral exciton and negative trion in the WS_2 monolayer. The atomic layer thickness causes a strong Columbic interaction between electrons and holes in the WS_2 monolayer.[12,30] Both neutral excitons and charged excitons exist with a high exciton density in monolayer WS_2.[47] Figure 4b further shows the Lorentz fitting of PL spectra at the positions marked as A–F in Figure 3c. Two peaks for neutral excitons and negative trions were used to subsequently understand the distinctive PL behaviors by the Lorentz fitting of PL spectra.[45,47−50] In particular, the contribution of trions in the PL in the 2H regions is greater than that in the 1T regions, which also verifies the essential difference between the 2H (semiconductor) phase and 1T (metal) phase.[26] In 1T/2H-WS_2 MLHSs, the PL intensity ratio of trions and excitons varies regularly with the alternating 1T and 2H phases, as shown in Figure 4c, implying the existence of completely different electronic states and the formation of MLHSs. Trions typically appear in the 2H phase, and there are more electrons that combine with excitons in that phase than in the 1T phase because of the direct band gap and associated inevitable defects;[34,47,49−51] thus, an obvious PL emission in the 2H phase is observed.

In addition, we discovered that the binding energy at positions B, D, and F is larger than that at positions A, C, and E when the binding energy of trions, defined as the peak energy difference between the exciton and trion, is calculated (Supporting Information, Figure S2c). Therefore, the charges are confined excitons in the plane, and the exciton binding energy is relatively large.[47−49] A higher binding energy suggests a higher carrier density in monolayer TMDs, as demonstrated elsewhere.[26,42,45,48] The higher carrier density is related to the formation of the 1T phase.[27,28,33,34]

We further used synchronous measurements of the surface morphology and surface potential to identify and understand MLHSs and their optical behaviors. The *in situ* atomic force microscopy (AFM) topography in Figure 5a displays

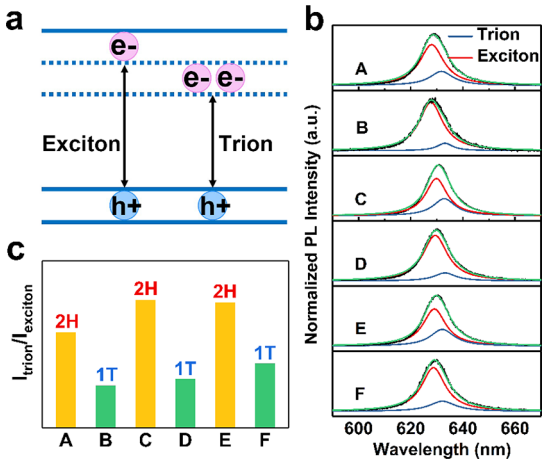

Figure 4. PL profiles of excitons and trions in a 2D MLHS with 1T/2H-WS_2. (a) Schematic diagram of excitons and trions in WS_2. (b) Lorentz fitting for excitons and trions in the PL curves in Figure 3b. (c) PL intensity ratio (trions/excitons) at positions A–F in the MLHSs in Figure 3c.

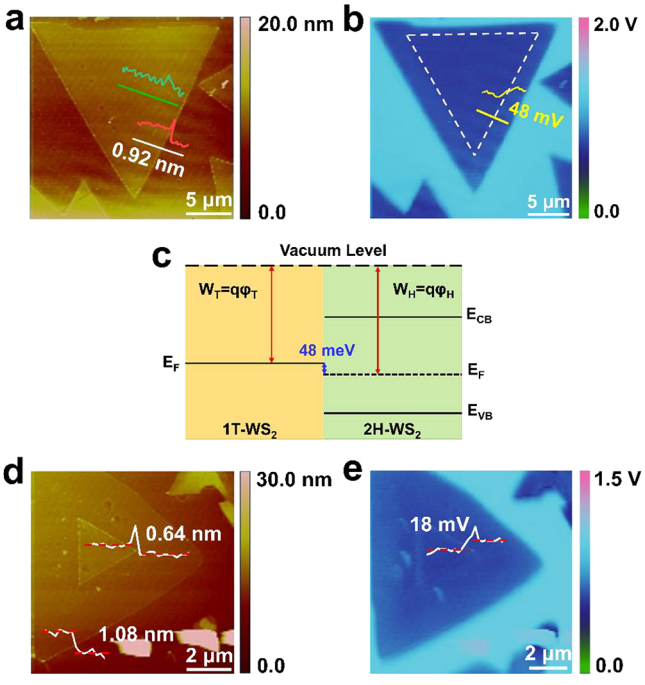

Figure 5. Surface morphology (AFM) and surface potential (KPFM) characterizations of 2D MLHSs with 1T/2H-WS_2. (a) Synchronous AFM and (b) KPFM images of the MLHS in Figure 3a. The surface potential interface is marked by a white dashed triangle. The contact potential difference (CPD) line profile is marked with a yellow line across the 2H-1T interface. (c) Energy band diagram for the 1T/2H-WS_2 superlattices in Figure 3a. (d) Synchronous AFM and (e) KPFM images of the 2D LHS in Figure 2a.

https://doi.org/10.1021/acsnano.1c07803
ACS Nano XXXX, XXX, XXX−XXX

monolayer WS_2 with a thickness of approximately 0.92 nm according to the white height line profile. In addition, the uniform height profile in the green line further reveals the formation of seamless 2D MLHSs.[30,33,41,52] Along the white dashed triangle, we observe that there is an obvious contact potential difference (V_{CPD}) or work function difference between the 1T and 2H phases in the corresponding Kelvin probe force microscopy (KPFM) image (Figure 5b). The surface potential of the 1T region is higher, and the surface potential difference is approximately 48 mV across the interface of the 1T and 2H domains, which is in congruence with the V_{CPD} reported in other literature.[32,36,43] Hence, charge transfer might occur from 1T regions to 2H regions, suggesting electronic doping. More electrons in the 2H regions are localized in the potential well formed by the MLHS structure with 1T/2H-WS_2. Thus, it is more likely to form trions and compound emission in the well.[45,48,49,53] Therefore, the PL emission is preferably produced in the 2H regions of MLHSs, while the PL intensity is higher than that previously observed in pure 2H-WS_2.[30,41,43] All of these results are in synchrony with the measurements and analyses above.

Figure 5c shows the energy band diagram for the 1T/2H-WS_2 lateral superlattice. The work function in the KPFM characterization is sensitive to the Fermi level of 2D materials.[54] Regarding the monolayer WS_2 with a stacked bilayer region in Figure 5d,e, the surface potential difference is merely approximately 18 mV between the WS_2 monolayer and bilayer. The AFM and KPFM characterizations further demonstrate that the periodic PL in monolayer WS_2 originates from MLHSs with alternating 1T and 2H phases and is independent of layer thickness or vertical stacking (Figure 5d,e). These investigations herald an exceptional vista of understanding and constructing MLHSs with anomalous optical and electronic behaviors. The analysis of PL behaviors demonstrates a simple route for further insights into the relationship between crystal structure and optical properties.[10,16]

CONCLUSIONS

We demonstrated MLHSs with alternating 1T and 2H domains in a WS_2 monolayer on a SiO_2/Si substrate. Periodic and localized PL emissions were explored through Raman spectroscopy, photoluminescence, KPFM characterization, and DFT calculations. The charge transport from the 1T to 2H regions, and their subsequent localization by the potential wells in MLHSs is responsible for the distinctive PL in 2H regions. While the PL dynamics and formation mechanism of MLHSs with 1T and 2H phases need more exploration, our studies create more opportunities for better understanding the phase engineering of a monolayer plane and for modulating the optical or electronic behavior of 2D materials in next-generation nanoscale optoelectronic devices.

METHODS

MLHSs were fabricated on SiO_2/Si substrates by using powdered WO_3 (99.9% purity, Sigma-Aldrich) and S (99.9% purity, Sigma-Aldrich) sources and adjusting the source temperature during a vapor−solid growth process. All procedures were based on the previous report.[54] Briefly, AFM and KPFM images were obtained on Veeco/DI multimode SPM, while optical microscopy was performed on Leica DM4000M. Raman and PL spectra and mapping were recorded on a Nanofinder 30 instrument (TII Tokyo Instruments, Inc.). An 1800 g/mm grating for Raman and a 300 g/mm grating for PL were used, while the measurements were performed with a 532 nm laser (0.02 mW and 0.015 mW) at room temperature.

ASSOCIATED CONTENT

Supporting Information

The Supporting Information is available free of charge at https://pubs.acs.org/doi/10.1021/acsnano.1c07803.

Raman spectra and PL for the 1T and 2H phases of WS_2; Raman position map of the E_{2g}^1 and A_{1g} phonon modes; variation of excitons and trions with alternating 1T and 2H phases according to the Lorentz fitting curves (PDF)

AUTHOR INFORMATION

Corresponding Authors

Xin Chen − *National Laboratory for Infrared Physics, Shanghai Institute of Technical Physics, Chinese Academy of Sciences, Shanghai 200083, China; Hangzhou Institute for Advanced Study, University of Chinese Academy of Sciences, Hangzhou 310024, China; University of Chinese Academy of Sciences, Beijing 100049, China;* orcid.org/0000-0001-7720-8916; Email: xinchen@mail.sitp.ac.cn

Zhiyong Fan − *Department of Electronic and Computer Engineering, The Hong Kong University of Science and Technology, Kowloon, Hong Kong SAR, China;* orcid.org/0000-0002-5397-0129; Email: eezfan@ust.hk

Guozhen Shen − *State Key Laboratory of Superlattices and Microstructures, Institute of Semiconductors, Chinese Academy of Sciences, Beijing 100083, China; University of Chinese Academy of Sciences, Beijing 100049, China;* orcid.org/0000-0002-9755-1647; Email: gzshen@semi.ac.cn

Authors

Wanli Yang − *National Laboratory for Infrared Physics, Shanghai Institute of Technical Physics, Chinese Academy of Sciences, Shanghai 200083, China; University of Chinese Academy of Sciences, Beijing 100049, China*

Tiantian Huang − *National Laboratory for Infrared Physics, Shanghai Institute of Technical Physics, Chinese Academy of Sciences, Shanghai 200083, China*

Junbo He − *National Laboratory for Infrared Physics, Shanghai Institute of Technical Physics, Chinese Academy of Sciences, Shanghai 200083, China*

Shuaijun Zhang − *National Laboratory for Infrared Physics, Shanghai Institute of Technical Physics, Chinese Academy of Sciences, Shanghai 200083, China*

Yan Yang − *National Laboratory for Infrared Physics, Shanghai Institute of Technical Physics, Chinese Academy of Sciences, Shanghai 200083, China*

Weiming Liu − *National Laboratory for Infrared Physics, Shanghai Institute of Technical Physics, Chinese Academy of Sciences, Shanghai 200083, China*

Xun Ge − *National Laboratory for Infrared Physics, Shanghai Institute of Technical Physics, Chinese Academy of Sciences, Shanghai 200083, China*

Rui Zhang − *National Laboratory for Infrared Physics, Shanghai Institute of Technical Physics, Chinese Academy of Sciences, Shanghai 200083, China*

Mengxia Qiu − *National Laboratory for Infrared Physics, Shanghai Institute of Technical Physics, Chinese Academy of Sciences, Shanghai 200083, China*

https://doi.org/10.1021/acsnano.1c07803
ACS Nano XXXX, XXX, XXX−XXX

Yuxiang Sang − *National Laboratory for Infrared Physics, Shanghai Institute of Technical Physics, Chinese Academy of Sciences, Shanghai 200083, China*
Xingjun Wang − *National Laboratory for Infrared Physics, Shanghai Institute of Technical Physics, Chinese Academy of Sciences, Shanghai 200083, China*
Xiaohao Zhou − *National Laboratory for Infrared Physics, Shanghai Institute of Technical Physics, Chinese Academy of Sciences, Shanghai 200083, China*
Tianxin Li − *National Laboratory for Infrared Physics, Shanghai Institute of Technical Physics, Chinese Academy of Sciences, Shanghai 200083, China*
Congfeng Liu − *National Laboratory for Infrared Physics, Shanghai Institute of Technical Physics, Chinese Academy of Sciences, Shanghai 200083, China*
Ning Dai − *National Laboratory for Infrared Physics, Shanghai Institute of Technical Physics, Chinese Academy of Sciences, Shanghai 200083, China; Hangzhou Institute for Advanced Study, University of Chinese Academy of Sciences, Hangzhou 310024, China; University of Chinese Academy of Sciences, Beijing 100049, China*

Complete contact information is available at: https://pubs.acs.org/10.1021/acsnano.1c07803

Notes

The authors declare no competing financial interest.

ACKNOWLEDGMENTS

This work was funded by the National Key R&D Program of China (2016YFA0202200), NSFC (92064014, 11933006), SCTSM (18J1414900) and Youth Innovation Promotion Association CAS. Z.F. acknowledges the support from the Center for 1D/2D Quantum Materials and the State Key Laboratory on Advanced Displays and Optoelectronics at HKUST.

REFERENCES

(1) Liu, Y.; Huang, Y.; Duan, X. van der Waals Integration before and beyond Two-Dimensional Materials. *Nature* **2019**, *567*, 323−333.
(2) Duan, X.; Wang, C.; Shaw, J. C.; Cheng, R.; Chen, Y.; Li, H.; Wu, X.; Tang, Y.; Zhang, Q.; Pan, A.; Jiang, J.; Yu, R.; Huang, Y.; Duan, X. Lateral Epitaxial Growth of Two-Dimensional Layered Semiconductor Heterojunctions. *Nat. Nanotechnol.* **2014**, *9*, 1024−1030.
(3) Han, G. H.; Duong, D. L.; Keum, D. H.; Yun, S. J.; Lee, Y. H. van der Waals Metallic Transition Metal Dichalcogenides. *Chem. Rev.* **2018**, *118*, 6297−6336.
(4) Zhang, Z.; Chen, P.; Duan, X.; Zang, K.; Luo, J.; Duan, X. Robust Epitaxial Growth of Two-Dimensional Heterostructures, Multiheterostructures, and Superlattices. *Science* **2017**, *357*, 788−792.
(5) Park, G.-H.; Nielsch, K.; Thomas, A. 2D Transition Metal Dichalcogenide Thin Films Obtained by Chemical Gas Phase Deposition Techniques. *Adv. Mater. Interfaces* **2019**, *6*, 1800688.
(6) Sahoo, P. K.; Memaran, S.; Xin, Y.; Balicas, L.; Gutierrez, H. R. One-Pot Growth of Two-Dimensional Lateral Heterostructures *via* Sequential Edge-Epitaxy. *Nature* **2018**, *553*, 63−67.
(7) Gong, Y.; Lin, J.; Wang, X.; Shi, G.; Lei, S.; Lin, Z.; Zou, X.; Ye, G.; Vajtai, R.; Yakobson, B. I.; Terrones, H.; Terrones, M.; Tay, B. K.; Lou, J.; Pantelides, S. T.; Liu, Z.; Zhou, W.; Ajayan, P. M. Vertical and In-Plane Heterostructures from WS_2/MoS_2 Monolayers. *Nat. Mater.* **2014**, *13*, 1135−1142.
(8) Zhou, K.; Jiang, J.; Ding, L. 2D Transition Metal Dichalcogenides for Neuromorphic Vision System. *J. Semicond.* **2021**, *42*, 090203.
(9) Chu, L.; Ding, L. Self-Assembled Monolayers in Perovskite Solar Cells. *J. Semicond.* **2021**, *42*, 090202.
(10) Dai, Z.; Hu, G.; Ou, Q.; Zhang, L.; Xia, F.; Garcia-Vidal, F. J.; Qiu, C. W.; Bao, Q. Artificial Metaphotonics Born Naturally in Two Dimensions. *Chem. Rev.* **2020**, *120*, 6197−6246.
(11) Meng, W.; Xu, F.; Yu, Z.; Tao, T.; Shao, L.; Liu, L.; Li, T.; Wen, K.; Wang, J.; He, L.; Sun, L.; Li, W.; Ning, H.; Dai, N.; Qin, F.; Tu, X.; Pan, D.; He, S.; Li, D.; Zheng, Y.; et al. Three-Dimensional Monolithic Micro-LED Display Driven by Atomically Thin Transistor Matrix. *Nat. Nanotechnol.* **2021**, *16*, 1231−1236.
(12) Huang, H. H.; Fan, X.; Singh, D. J.; Zheng, W. T. Recent Progress of TMD Nanomaterials: Phase Transitions and Applications. *Nanoscale* **2020**, *12*, 1247−1268.
(13) Kappera, R.; Voiry, D.; Yalcin, S. E.; Branch, B.; Gupta, G.; Mohite, A. D.; Chhowalla, M. Phase-Engineered Low-Resistance Contacts for Ultrathin MoS_2 Transistors. *Nat. Mater.* **2014**, *13*, 1128−1134.
(14) Wang, J.; Li, Z.; Chen, H.; Deng, G.; Niu, X. Recent Advances in 2D Lateral Heterostructures. *Nano-Micro Lett.* **2019**, *11*, 48.
(15) Li, T.; Guo, W.; Ma, L.; Li, W.; Yu, Z.; Han, Z.; Gao, S.; Liu, L.; Fan, D.; Wang, Z.; Yang, Y.; Lin, W.; Luo, Z.; Chen, X.; Dai, N.; Tu, X.; Pan, D.; Yao, Y.; Wang, P.; Nie, Y.; et al. Epitaxial Growth of Wafer-Scale Molybdenum Disulfide Semiconductor Single Crystals on Sapphire. *Nat. Nanotechnol.* **2021**, *16*, 1201−1207.
(16) Li, Z.; Zheng, J.; Zhang, Y.; Zheng, C.; Woon, W. Y.; Chuang, M. C.; Tsai, H. C.; Chen, C. H.; Davis, A.; Xu, Z. Q.; Lin, J.; Zhang, H.; Bao, Q. Synthesis of Ultrathin Composition Graded Doped Lateral WSe_2/WS_2 Heterostructures. *ACS Appl. Mater. Interfaces* **2017**, *9*, 34204−34212.
(17) Nourbakhsh, A.; Zubair, A.; Sajjad, R. N.; Tavakkoli K. G., A.; Chen, W.; Fang, S.; Ling, X.; Kong, J.; Dresselhaus, M. S.; Kaxiras, E.; Berggren, K. K.; Antoniadis, D.; Palacios, T. MoS_2 Field-Effect Transistor with Sub-10 nm Channel Length. *Nano Lett.* **2016**, *16*, 7798−7806.
(18) Thakur, D.; Kumar, P.; Balakrishnan, V. Phase Selective CVD Growth and Photoinduced 1T → 1H Phase Transition in a WS_2 Monolayer. *J. Mater. Chem. C* **2020**, *8*, 10438−10447.
(19) Lin, Y. C.; Dumcenco, D. O.; Huang, Y. S.; Suenaga, K. Atomic Mechanism of the Semiconducting-to-Metallic Phase Transition in Single-Layered MoS_2. *Nat. Nanotechnol.* **2014**, *9*, 391−396.
(20) Sung, J. H.; Heo, H.; Si, S.; Kim, Y. H.; Noh, H. R.; Song, K.; Kim, J.; Lee, C. S.; Seo, S. Y.; Kim, D. H.; Kim, H. K.; Yeom, H. W.; Kim, T. H.; Choi, S. Y.; Kim, J. S.; Jo, M. H. Coplanar Semiconductor-Metal Circuitry Defined on Few-Layer $MoTe_2$ *via* Polymorphic Heteroepitaxy. *Nat. Nanotechnol.* **2017**, *12*, 1064−1070.
(21) Xu, X.; Liu, S.; Han, B.; Han, Y.; Yuan, K.; Xu, W.; Yao, X.; Li, P.; Yang, S.; Gong, W.; Muller, D. A.; Gao, P.; Ye, Y.; Dai, L. Scaling-up Atomically Thin Coplanar Semiconductor-Metal Circuitry *via* Phase Engineered Chemical Assembly. *Nano Lett.* **2019**, *19*, 6845−6852.
(22) Tan, C.; Wang, H.; Zhu, X.; Gao, W.; Li, H.; Chen, J.; Li, G.; Chen, L.; Xu, J.; Hu, X.; Li, L.; Zhai, T. A Self-Powered Photovoltaic Photodetector Based on a Lateral WSe_2-WSe_2 Homojunction. *ACS Appl. Mater. Interfaces* **2020**, *12*, 44934−44942.
(23) Kochat, V.; Apte, A.; Hachtel, J. A.; Kumazoe, H.; Krishnamoorthy, A.; Susarla, S.; Idrobo, J. C.; Shimojo, F.; Vashishta, P.; Kalia, R.; Nakano, A.; Tiwary, C. S.; Ajayan, P. M. Re Doping in 2D Transition Metal Dichalcogenides as a New Route to Tailor Structural Phases and Induced Magnetism. *Adv. Mater.* **2017**, *29*, 1703754.
(24) Cho, S.; Kim, S.; Kim, J. H.; Zhao, J.; Seok, J.; Keum, D. H.; Baik, J.; Choe, D.-H.; Chang, K. J.; Suenaga, K.; Kim, S. W.; Lee, Y. H.; Yang, H. Phase Patterning for Ohmic Homojunction Contact in $MoTe_2$. *Science* **2015**, *349*, 625−628.
(25) Wang, R.; Yu, Y.; Zhou, S.; Li, H.; Wong, H.; Luo, Z.; Gan, L.; Zhai, T. Strategies on Phase Control in Transition Metal Dichalcogenides. *Adv. Funct. Mater.* **2018**, *28*, 1802473.
(26) Wilson, J. A.; Yoffe, A. D. The Transition Metal Dichalcogenides Discussion and Interpretation of the Observed

Optical, Electrical and Structural Properties. *Adv. Phys.* **1969**, *18*, 193−335.
(27) Eda, G.; Fujita, T.; Yamaguchi, H.; Voiry, D.; Chen, M.; Chhowalla, M. Coherent Atomic and Electronic Heterostructures of Single-Layer MoS_2. *ACS Nano* **2012**, *6*, 7311.
(28) Enyashin, A. N.; Yadgarov, L.; Houben, L.; Popov, I.; Weidenbach, M.; Tenne, R.; Bar-Sadan, M.; Seifert, G. New Route for Stabilization of 1T-WS_2 and MoS_2 Phases. *J. Phys. Chem. C* **2011**, *115*, 24586−24591.
(29) Kim, M. S.; Yun, S. J.; Lee, Y.; Seo, C.; Han, G. H.; Kim, K. K.; Lee, Y. H.; Kim, J. Biexciton Emission from Edges and Grain Boundaries of Triangular WS_2 Monolayers. *ACS Nano* **2016**, *10*, 2399−2405.
(30) Ren, D.-D.; Qin, J.-K.; Li, Y.; Miao, P.; Sun, Z.-Y.; Xu, P.; Zhen, L.; Xu, C.-Y. Photoluminescence Inhomogeneity and Excitons in CVD-Grown Monolayer WS_2. *Opt. Mater.* **2018**, *80*, 203−208.
(31) Hu, Z.; Avila, J.; Wang, X.; Leong, J. F.; Zhang, Q.; Liu, Y.; Asensio, M. C.; Lu, J.; Carvalho, A.; Sow, C. H.; Castro Neto, A. H. The Role of Oxygen Atoms on Excitons at the Edges of Monolayer WS_2. *Nano Lett.* **2019**, *19*, 4641−4650.
(32) Kastl, C.; Koch, R. J.; Chen, C. T.; Eichhorn, J.; Ulstrup, S.; Bostwick, A.; Jozwiak, C.; Kuykendall, T. R.; Borys, N. J.; Toma, F. M.; Aloni, S.; Weber-Bargioni, A.; Rotenberg, E.; Schwartzberg, A. M. Effects of Defects on Band Structure and Excitons in WS_2 Revealed by Nanoscale Photoemission Spectroscopy. *ACS Nano* **2019**, *13*, 1284−1291.
(33) Lin, Y. C.; Yeh, C. H.; Lin, H. C.; Siao, M. D.; Liu, Z.; Nakajima, H.; Okazaki, T.; Chou, M. Y.; Suenaga, K.; Chiu, P. W. Stable 1T Tungsten Disulfide Monolayer and Its Junctions: Growth and Atomic Structures. *ACS Nano* **2018**, *12*, 12080−12088.
(34) Chen, M.; Ji, B.; Dai, Z.; Du, X.; He, B.; Chen, G.; Liu, D.; Chen, S.; Lo, K. H.; Wang, S.; Zhou, B.; Pan, H. Vertically-Aligned 1T/2H-MS_2 (M = Mo, W) Nanosheets for Surface-Enhanced Raman Scattering with Long-Term Stability and Large-Scale Uniformity. *Appl. Surf. Sci.* **2020**, *527*, 146769.
(35) Melitz, W.; Shen, J.; Kummel, A. C.; Lee, S. Kelvin Probe Force Microscopy and Its Application. *Surf. Sci. Rep.* **2011**, *66*, 1−27.
(36) Kumar, P.; Biswas, J.; Pandey, J.; Thakar, K.; Soni, A.; Lodha, S.; Balakrishnan, V. Selective Oxidation of WS_2 Defect Domain with Sub-Monolayer Thickness Leads to Multifold Enhancement in Photoluminescence. *Adv. Mater. Interfaces* **2019**, *6*, 1900962.
(37) Zhang, Z.; Gong, Y.; Zou, X.; Liu, P.; Yang, P.; Shi, J.; Zhao, L.; Zhang, Q.; Gu, L.; Zhang, Y. Epitaxial Growth of Two-Dimensional Metal-Semiconductor Transition-Metal Dichalcogenide Vertical Stacks (VSe_2/MX_2) and Their Band Alignments. *ACS Nano* **2019**, *13*, 885−893.
(38) Zhu, J.; Li, W.; Huang, R.; Ma, L.; Sun, H.; Choi, J. H.; Zhang, L.; Cui, Y.; Zou, G. One-Pot Selective Epitaxial Growth of Large WS_2/MoS_2 Lateral and Vertical Heterostructures. *J. Am. Chem. Soc.* **2020**, *142*, 16276−16284.
(39) Liu, J.; Lo, T. W.; Sun, J.; Yip, C. T.; Lam, C. H.; Lei, D. Y. A Comprehensive Comparison Study on the Vibrational and Optical Properties of CVD-Grown and Mechanically Exfoliated Few-Layered WS_2. *J. Mater. Chem. C* **2017**, *5*, 11239−11245.
(40) He, Z.; Sheng, Y.; Rong, Y.; Lee, G.-D.; Li, J.; Warner, J. H. Layer-Dependent Modulation of Tungsten Disulfide Photoluminescence by Lateral Electric Fields. *ACS Nano* **2015**, *9*, 2740−2748.
(41) Cong, C.; Shang, J.; Wu, X.; Cao, B.; Peimyoo, N.; Qiu, C.; Sun, L.; Yu, T. Synthesis and Optical Properties of Large-Area Single-Crystalline 2D Semiconductor WS_2 Monolayer from Chemical Vapor Deposition. *Adv. Opt. Mater.* **2014**, *2*, 131−136.
(42) Li, T.; Li, M.; Lin, Y.; Cai, H.; Wu, Y.; Ding, H.; Zhao, S.; Pan, N.; Wang, X. Probing Exciton Complexes and Charge Distribution in Inkslab-Like WSe_2 Homojunction. *ACS Nano* **2018**, *12*, 4959−4967.
(43) Kumar, P.; Thakar, K.; Verma, N. C.; Biswas, J.; Maeda, T.; Roy, A.; Kaneko, K.; Nandi, C. K.; Lodha, S.; Balakrishnan, V. Polymorphic In-Plane Heterostructures of Monolayer WS_2 for Light-Triggered Field-Effect Transistors. *ACS Appl. Nano Mater.* **2020**, *3*, 3750−3759.
(44) Zhang, X.; Jin, Z.; Wang, L.; Hachtel, J. A.; Villarreal, E.; Wang, Z.; Ha, T.; Nakanishi, Y.; Tiwary, C. S.; Lai, J.; Dong, L.; Yang, J.; Vajtai, R.; Ringe, E.; Idrobo, J. C.; Yakobson, B. I.; Lou, J.; Gambin, V.; Koltun, R.; Ajayan, P. M. Low Contact Barrier in 2H/1T' $MoTe_2$ In-Plane Heterostructure Synthesized by Chemical Vapor Deposition. *ACS Appl. Mater. Interfaces* **2019**, *11*, 12777−12785.
(45) Mitioglu, A. A.; Plochocka, P.; Jadczak, J. N.; Escoffier, W.; Rikken, G. L. J. A.; Kulyuk, L.; Maude, D. K. Optical Manipulation of the Exciton Charge State in Single-Layer Tungsten Disulfide. *Phys. Rev. B: Condens. Matter Mater. Phys.* **2013**, *88*, 245403.
(46) Ding, W.; Hu, L.; Liu, Q. C.; Sheng, Z. G.; Dai, J. M.; Zhu, X. B.; Sun, Y. P. Structure Modulation Induced Enhancement of Microwave Absorption in WS_2 Nanosheets. *Appl. Phys. Lett.* **2018**, *113*, 243102.
(47) Plechinger, G.; Nagler, P.; Kraus, J.; Paradiso, N.; Strunk, C.; Schüller, C.; Korn, T. Identification of Excitons, Trions and Biexcitons in Single-Layer WS_2. *Phys. Status Solidi RRL* **2015**, *9*, 457−461.
(48) Mak, K. F.; He, K.; Lee, C.; Lee, G. H.; Hone, J.; Heinz, T. F.; Shan, J. Tightly Bound Trions in Monolayer MoS_2. *Nat. Mater.* **2013**, *12*, 207−211.
(49) Chernikov, A.; Berkelbach, T. C.; Hill, H. M.; Rigosi, A.; Li, Y.; Aslan, O. B.; Reichman, D. R.; Hybertsen, M. S.; Heinz, T. F. Exciton Binding Energy and Nonhydrogenic Rydberg Series in Monolayer WS_2. *Phys. Rev. Lett.* **2014**, *113*, 076802.
(50) Zhu, B.; Chen, X.; Cui, X. Exciton Binding Energy of Monolayer WS_2. *Sci. Rep.* **2015**, *5*, 9218.
(51) Tsai, T. H.; Liang, Z. Y.; Lin, Y. C.; Wang, C. C.; Lin, K. I.; Suenaga, K.; Chiu, P. W. Photogating WS_2 Photodetectors Using Embedded WSe_2 Charge Puddles. *ACS Nano* **2020**, *14*, 4559−4566.
(52) Liu, H.; Lu, J.; Ho, K.; Hu, Z.; Dang, Z.; Carvalho, A.; Tan, H. R.; Tok, E. S.; Sow, C. H. Fluorescence Concentric Triangles: A Case of Chemical Heterogeneity in WS_2 Atomic Monolayer. *Nano Lett.* **2016**, *16*, 5559−5567.
(53) van der Zande, A. M.; Huang, P. Y.; Chenet, D. A.; Berkelbach, T. C.; You, Y.; Lee, G. H.; Heinz, T. F.; Reichman, D. R.; Muller, D. A.; Hone, J. C. Grains and Grain Boundaries in Highly Crystalline Monolayer Molybdenum Disulphide. *Nat. Mater.* **2013**, *12*, 554−561.
(54) Zhang, K.; Zhang, T.; Cheng, G.; Li, T.; Wang, S.; Wei, W.; Zhou, X.; Yu, W.; Sun, Y.; Wang, P.; Zhang, D.; Zeng, C.; Wang, X.; Hu, W.; Fan, H. J.; Shen, G.; Chen, X.; Duan, X.; Chang, K.; Dai, N. Interlayer Transition and Infrared Photodetection in Atomically Thin Type-II $MoTe_2/MoS_2$ van der Waals Heterostructures. *ACS Nano* **2016**, *10*, 3852−3858.

https://doi.org/10.1021/acsnano.1c07803
ACS Nano XXXX, XXX, XXX−XXX